ADVANCED MATERIALS INTERFACES
www.advmatinterfaces.de

Characterization of the Coupling between Out-of-Plane Graphene and Electrogenic Cells

*Laura Matino, Sahil K. Rastogi, Leonardo D. Garma, Tzahi Cohen-Karni, and Francesca Santoro**

The cell-chip coupling is in general regulated by the interplay between cells and the material surface at the interface. Electroactive planar materials have shown limited crosstalk with cells, whereas pseudo 3D patterned materials promote a more intimate contact with the biological system. Here, unprecedented physical properties of a carbon-based material, i.e., graphene, to engineer out-of-plane morphologies are exploited: 1) 3D single- to few-layer fuzzy graphene morphology (3DFG), 2) 3DFG on a collapsed Si nanowire mesh template, and 3) 3DFG on a noncollapsed Si nanowire mesh template. These materials are synthesized and interfaced with cardiomyocyte-like cells focusing on the characterization of the cytoskeletal arrangement as well as membrane wrapping processes yet regulated by endocytic proteins. Finally, some major conditions to promote tight coupling to the device and eventually spontaneous intracellular penetration are found.

Bioelectronic platforms directly interface biological systems to transduce cellular processes into processable electronic signals or modulate cellular functionalities through electrical fields. Recent studies have revealed how the adhesion between cells and the electroactive material plays a pivotal role to enhance the cell–chip coupling and recording/stimulating performance of the devices.[1–3] Among several approaches, the surface engineering with out-of-plane micro and nanostructures has led to promote adhesion as well as phagocytosis-like processes at the cell–material interface.[4] In turn, those topographies as well as more complex mesh-like electroactive material surfaces can resemble curvatures and geometries present in living tissues, recapitulate the native cell environment and, ultimately, trigger an optimal integration of cells with the bioelectronic device. In parallel, carbon-based materials have been explored for their unique physical and chemical properties along with their electrical conductivity.[5] Among all, graphene has been employed for various in vivo and in vitro bioelectronics applications[6,7] and has been shown to be suitable for electrophysiology investigation of 2D and 3D electrogenic cells cultures,[8–10] and for influencing the transmission of the electrical signal across a cell network.[11] However, the main applications of graphene still rely on 2D conformations where the intrinsic bulk arrangement of the material might not be optimal for the effective cell–chip coupling. In this scenario, we explored how to vary the curvature of graphene at the interface with electrogenic cells through the synthesis of out-of-plane architectures. In fact, these morphologies could either induce local high curvature and membrane deformation and ultimately locally trigger spontaneous penetration intracellularly.

Here, we investigated the response of cardiomyocyte-like cells on to three graphene topologies: 1) 3D single- to few-layer fuzzy graphene (3DFG), 2) 3DFG on a collapsed Si nanowire (SiNW) mesh template (NT-3DFGc), and 3) 3DFG on a noncollapsed Si nanowire mesh template (NT-3DFGnc). We evaluated the effect of the newly synthesized materials on cells' viability and electrical activity, adhesion, and spreading by fluorescence labeling of peculiar cytoskeletal components. We characterized curvature-sensitive proteins related to endocytic processes and membrane conformation at the nanoscale to evaluate possible spontaneous penetration mechanism and cell–chip coupling.

We fabricated i) 2D planar graphene (2DG), ii) 3DFG, iii) NT-3DFGc, and iv) NT-3DFGnc. 2DG and 3DFG were synthesized using low pressure chemical vapor deposition (LPCVD),[12] and plasma-enhanced chemical vapor deposition (PECVD) method,[13] respectively. 3DFG was further deposited on collapsed Si nanowire mesh and noncollapsed Si nanowire templates to obtain NT-3DFGc and NT-3DFGnc, respectively (see the Experimental Section). The morphology of the different graphene-based materials was investigated via scanning electron

L. Matino, Dr. L. D. Garma,[+] Dr. F. Santoro
Tissue Electronics
Istituto Italiano di Tecnologia
Naples 80125, Italy
E-mail: francesca.santoro@iit.it
L. Matino
Dipartimento di Ingegneria Chimica
dei Materiali e delle Produzioni Industriali
DICMAPI
Università 'Federico II'
Naples 80125, Italy
Dr. S. K. Rastogi, Dr. T. Cohen-Karni
Department of Biomedical Engineering
Carnegie Mellon University
Pittsburgh, PA 15213, USA
Dr. T. Cohen-Karni
Department of Materials Science and Engineering
Carnegie Mellon University
Pittsburgh, PA 15213, USA
The ORCID identification number(s) for the author(s) of this article can be found under https://doi.org/10.1002/admi.202000699.
[+]Present address: Laboratory of Molecular Neurobiology, Department of Medical Biochemistry and Biophysics, Karolinska Institute, Stockholm SE-17177, Sweden

DOI: 10.1002/admi.202000699

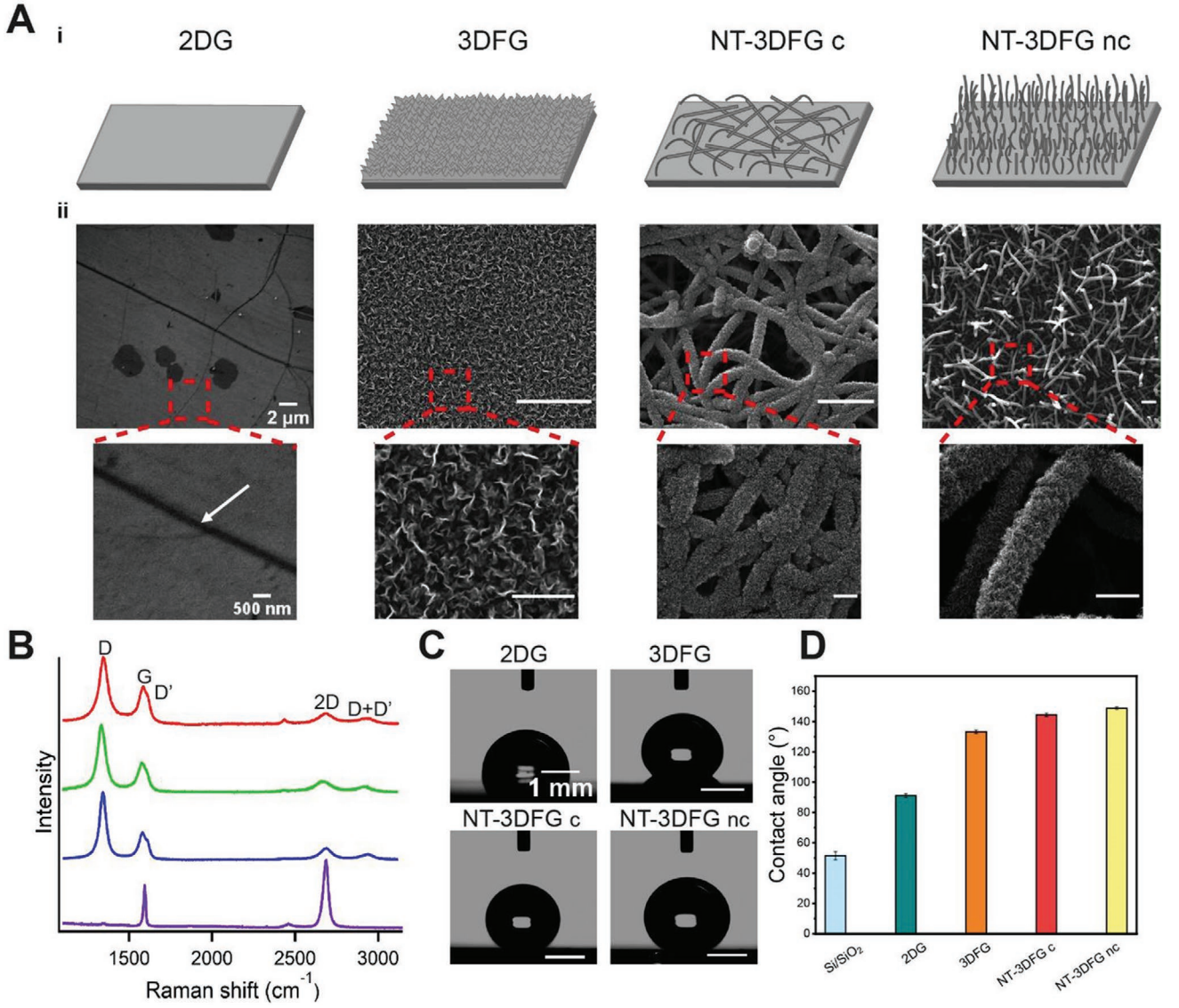

Figure 1. Graphene-based substrates with diverse topographies. A) Schematic (i) and scanning electron microscopy images (ii) of different graphene topographies. B) Exemplary Raman spectra of 2DG (violet), 3DFG (blue), NT-3DFGc (green), and NT-3DFGnc (red). C) Contact angle measurement images and D) contact angle quantification of Si/SiO_2, 2DG, 3DFG, NT-3DFGc, and NT-3DFGnc substrates. Results are presented as mean ± SD ($N = 3$). Si/SiO_2 substrates were considered as control sample.

microscopy (SEM) as shown in **Figure 1**A. A typical planar morphology was identified in the case of the synthesized 2DG (the white arrow in Figure 1Aii represents the grain boundary) while out-of-plane architectures were obtained for 3DFG and both NT-3DFG templates (Figure 1). During the 3DFG synthesis, graphene flakes were deposited on a planar surface resulting in a roughness at the sub-micrometer scale (464 ± 25 nm). Instead, collapsed and noncollapsed nanowires in NT-3DFG templates lead to sub-micro- and nanometric topography due to Si nanowire core size and graphene flakes coverage, respectively.

Furthermore, the composition of the flakes was investigated using Raman spectroscopy (Figure 1B). The presence of a sharp G peak at ≈1580 cm^{-1}, a symmetric 2D peak at ≈2700 cm^{-1} with full width at half-maximum (FWHM) of ≈40 cm^{-1}, and no significant D peak at ≈1340 cm^{-1}, in the 2DG spectrum confirms presence of defect-free monolayer graphene.[12] The emergence of the D peak, and the D′ peak, as a shoulder to the G peak, in the spectra for 3DFG and NT-3DFG is attributed to the breaks in translational symmetry due to the presence of graphene edges.[13] The number of graphene layers can be determined by investigating the shape as well as the number of Lorentzian peaks that can be fitted in the 2D peak.[14] For 3DFG and NT-3DFG, the presence of a broad and symmetric 2D peak that can be fitted with a single Lorentzian, suggests the presence of juxtaposed single- to few-layer graphene flakes.[13]

The morphology of graphene also affected the surface physical properties of the substrates as revealed by the surface wettability characterization using contact angle measurements (Figure 1C,D). 3DFG materials show super hydrophobic behavior ($\theta \approx 133°$) as compared to Si/SiO_2 ($\theta \approx 51°$) and 2DG

substrates ($\theta \approx 90°$). The superhydrophobicity is attributed to the presence of air pockets between the graphene flakes as explained by the Cassie–Baxter model of porous surface wettability.[15,16] An increase in the porosity due to the presence of micropores in the NT-3DFG substrates, as evident in the SEM image (Figure 1A), further leads to more air pockets and thus higher hydrophobicity ($\theta \approx 145°$).

Then, HL-1 cells were cultured on the graphene-based materials and control samples (Si/SiO_2) after surface functionalization (see the Experimental Section). The newly synthesized materials' biocompatibility was evaluated through a fluorescence vitality assay (see the Experimental Section) where live and dead cells were labeled with Calcein-AM (green fluorescence signal in **Figure 2**A) and propidium iodide (red fluorescence signal in Figure 2A), respectively. Results related to Si/SiO_2 substrates are reported in Figure S1 (Supporting Information). Hence, cell viability was quantified as shown in Figure 2B. NT-3DFGnc exhibited a smaller population of living cells (over 88% in average, $N = 3$) compared to the other materials (over 90% in average, $N = 3$, for 2DG, 3DFG, and NT-3DFGc), probably due to the piercing effect that single free-standing nanowire or their clusters may cause to the cell membrane, thereby facilitating cell cytosol and homeostasis loss. Furthermore, all the graphene-based materials displayed negligible cytotoxic effects on HL-1 cells as also reported in previous results.[12,17]

To further validate that out-of-plane graphene materials do not affect cells' functionalities, we evaluated the Ca^{2+} flow across a confluent monolayer of HL-1 cells (see Figures S2–S4, Supporting Information).

To investigate in details the effective coupling between cells and the diverse graphene materials, HL-1 cells were plasticized on 2DG, 3DFG, NT-3DFGc, and NT-3DFGnc following the previously reported ultrathin plasticization embedding

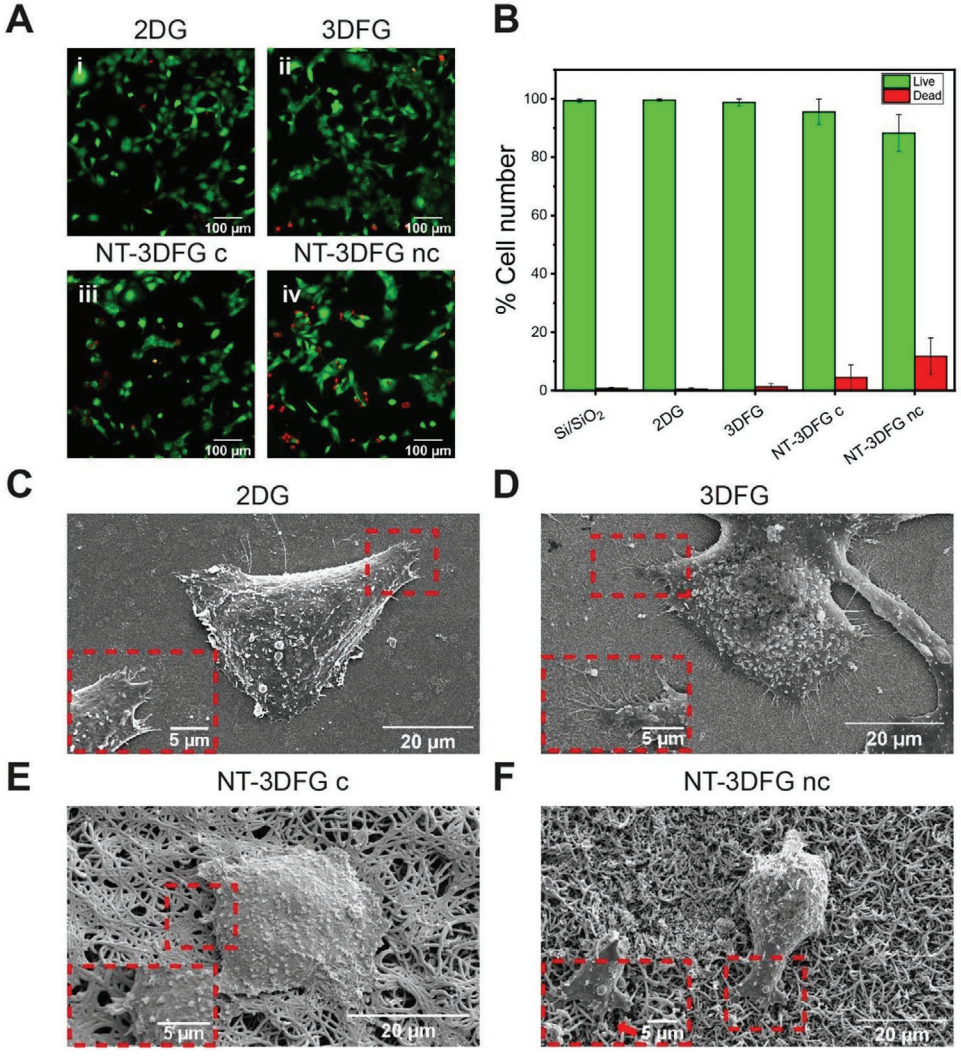

Figure 2. Biocompatibility assessment and electron microscopy of HL-1 cells cultured on planar and out-of-plane graphene materials and Ca^{2+} wave propagation velocity assay. A) Cell vitality assay through live (green) and dead (red) cell labeling with Calcein AM and propidium iodide, respectively. B) Percentage of live and dead cell represented as mean ± SD ($N = 3$). Scanning electron microscopy images of plasticized cells on C) 2DG graphene (top view, secondary electrons), D) 3DFG graphene (top view, secondary electrons), E) NT 3DFGc graphene (top view, secondary electrons), and F) NT 3DFGnc (top view, secondary electrons).

method.[18,19] Here, both graphene and cells' structures were preserved by the resin inclusion and SEM were acquired to visualize the physical interaction between the material surface and cells as shown in Figure 2C–F (additional cross sections are shown in Figure S5, Supporting Information). SEM of cells on Si/SiO_2 are shown in Figure S6 (Supporting Information).

Top view micrographs reveal how HL-1 cells spread and form protrusions, i.e., filopodia, when in contact with the different graphene-based materials, as shown in the insets in Figure 2C–F. These membrane extensions represent local junctional points and cell spatial sensors capable of collecting information from the surrounding environment.[20] Here, thicker and straight filopodia were visible in cells cultured on 2DG and the interaction with the substrate was limited to the close proximity of the cell body. In contrast, membrane protrusions on 3DFG resulted rather thinner and longer (extending the cell–material interaction to an area distant from the cell body (Figure 2D)). Few filopodia were visible when cell adhered on NT-3DFGc, having a similar thick and short morphology as depicted in the planar graphene configuration (Figure 2E). Finally, fewer thicker and bent protrusions wrapped single free-standing nanowires of NT-3DFGnc (Figure 2F). These findings are in accordance with similar studies reporting on how out-of-plane structures improve the cell–material coupling since they provide anchorage sites for cells.[21,22]

To further investigate the cellular response to the surface topography of the out-of-plane materials, cells were fluorescently labeled by targeting nuclei, F-actin, and paxillin proteins after 1 DIV. From confocal images (**Figure 3**A,B) showing the distribution of F-actin and paxillin proteins, we identified thicker actin bundles in HL-1 cells cultured on planar 2DG (labeling related to control substrates is shown in Figure S8, Supporting Information) and 3DFG materials suggesting the formation of a randomly organized robust actin network (Figure 3A v,vi and Figure 3B i,ii). NT-3DFG collapsed and noncollapsed graphene wires impaired the maturation of strong fibers, promoting actin accumulation at cell–wires contact points, as shown in Figure 3B iii,iv, for NT-3DFGc and NT-3DFGnc, respectively, and also confirmed by the lower fluorescence intensity level measured in Figure 3C. In this case, F-actin accumulation suggests that the high curvature of the plasma membrane at the interface with the wires could trigger curvature-sensitive domains as also demonstrated for cells grown on vertical nanostructures which might exert an overall downregulation of the gene-level expression of both F-actin and FAs protein components.[21,23–26]

In addition, paxillin proteins show a large patch conformation at the end of actin fibers when cells were interfaced with 3DFG and 2DG as evidence of mature focal adhesion (FA) proteins as shown in Figure 3A ii and i, respectively.[25] In contrast, NT-3DFGc and NT-3DFGnc templates drastically influence focal adhesion protein development as no clear patches were identified but rather a diffused distribution at the cell body area (Figure 3A iii and iv, respectively), which might be a consequence of the adhesion mainly arising at the tips of the wires. The paxillin expression was also confirmed by the fluorescence intensity quantification shown in Figure 3D.

Moreover, cellular attachment was characterized through specific cell shape descriptors, i.e., area, cell elongation, cell circularity, and minor and major cell axis lengths quantification (Figure 3E–G and Figure S7, Supporting Information). Here, HL-1 cells show an average area on 3DFG graphene almost twofold higher than on NT-3DFGc and NT-3DFGnc as shown in Figure 3E (cell area values are reported in Section S7, Supporting Information). Although the nanowires were highly dense synthesized in both NT-3DFG c and NT-3DFG nc, the overall attachment area might not foster an extensive spread. From the analysis of cell elongation (A_{MIN}/A_{MAX}), circularity and cell axis lengths (shown in Figure 3F,G, and Figure S7, Supporting Information, respectively), we found no specific cell polarization due to the random distribution of wires of out-of-plane materials while longer axis were found for HL-1 cultured on both 2DG and 3DFG. Therefore, taken together, the cell shape descriptors suggest that planar and 3DFG promote HL-1 spreading and stretching out, on the contrary when interfaced with NT-3DFGc and nc templates HL-1 remained round and small.

Our data suggest a significant role that cell membrane and transmembrane proteins have in regulating the interaction between HL-1 cells and graphene-based planar and out-of-plane materials. In this context, the F-actin distribution reflects a more structured cytoskeleton organization on the larger adhesion area stabilized by mature focal adhesion proteins in cells cultured on 3DFG substrates. In contrast, cells on wire-based graphene substrates exhibit F-actin accumulation in correspondence of the wires and weak adhesion points.

Effectively, the cell directly mediates the interaction with the material underneath through specific adhesion proteins,[27] and the plasma membrane deforms according to the local curvature induced by the diverse material topographies.[18,19,23]

As previously reported, the material curvature might trigger characteristic budding of the membrane to form endocytic invaginations and vesicles.[23,28] Therefore, the contact area between the plasma membrane and the graphene substrates has been further investigated through SEM and in situ cross sectioning achieved by focused ion beam (FIB) milling.

We identified membrane invaginations (**Figure 4**A–D) in the range of 50–200 nm (diameter) which are typical of endocytosis processes mediated by clathrin and caveolin-1 proteins.[28,29] In particular, in the presence of fiber-like graphene, as found in NT-3DFGc, clear membrane wrapping events develop around single fibers (Figure 4C). Finally, in the case of NT-3DFGnc, several wires have been found in the cytosol and no clear membrane components have been identified around the wires (Figure 4D). This suggests that sporadic spontaneous membrane poration could be achieved.

These potential penetration events were further characterized through fluorescent labeling of topography-related internalization pathways. As previous works have reported,[23,28,30] nano and microstructured surfaces might provide for local membrane curvature pinning and triggering curvature-sensitive proteins recruitment, such as clathrin and caveolin-1. Consequently, we evaluated the fluorescence intensity of these proteins (Figure 4E–G) considering confocal images of the cell membrane area in contact with the diverse substrates. According to the intensity profiles, we found that HL-1 cultured on out-of-plane structures exhibited a higher clathrin and cav-1 fluorescence signal than cells in contact with 2DG (as well as

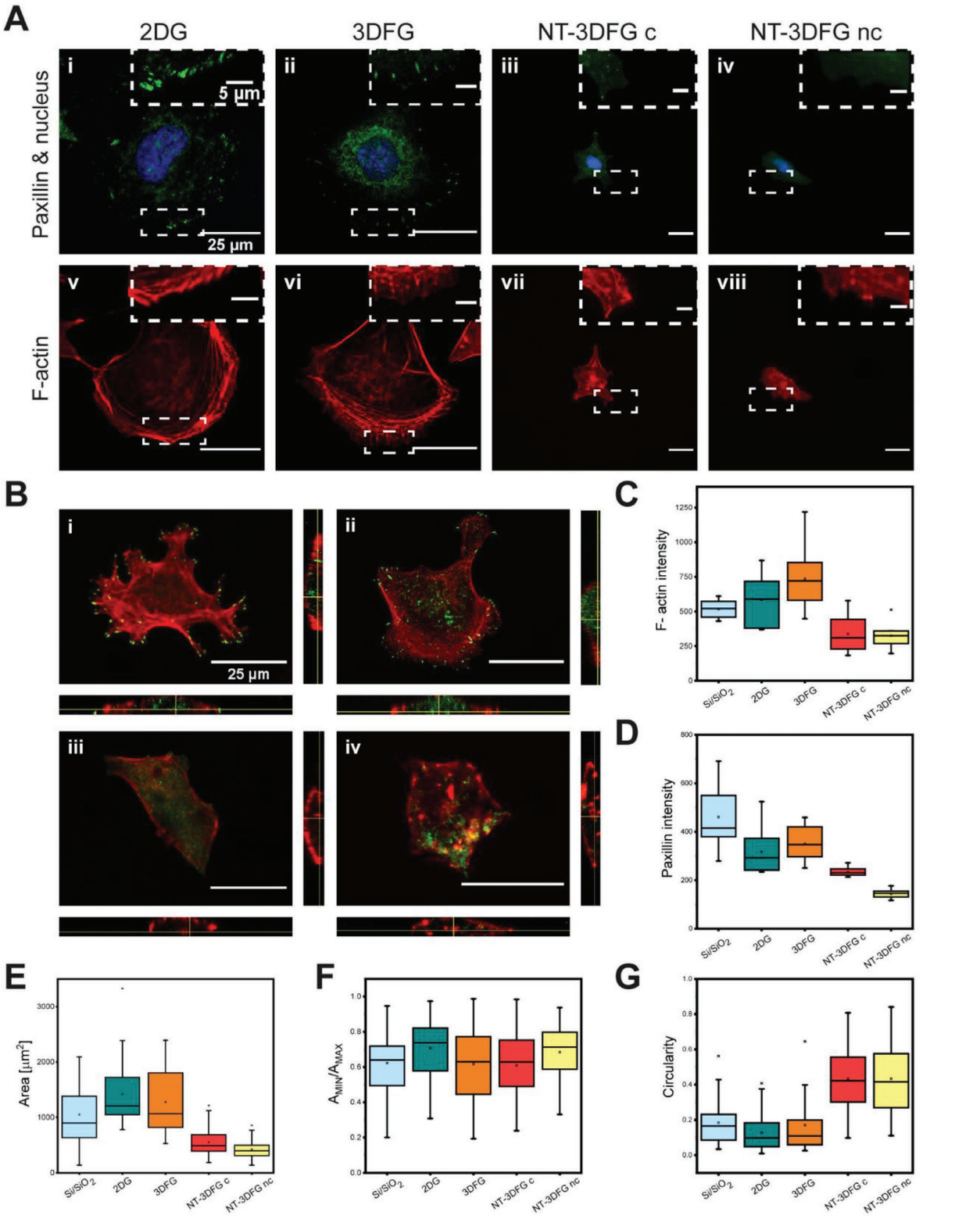

Figure 3. Adhesion and spreading through fluorescence microscopy. A) Fluorescence images of cells on 2DG (i, v), 3DFG (ii, vi), NT-3DFG c (iii, vii), and NT-3DFG nc (iv, viii), where paxillin proteins were labeled in green, F-actin in red, and nuclei in blue. B) Z-stack fluorescence images (*xy* plane) and optical cross sections (bottom *xz* plane, right *yz* plane) of HL-1 on 2DG (i) with 5.56 µm thickness, 3DFG (ii) with 5 µm thickness, NT-3DFG c (iii) with 7 µm-thickness, and NT-3DFG nc (iv) with 10.92 µm thickness. Paxillin proteins were labeled in green and F-actin in red. Scale bar is 25 µm. Quantification of C) F-actin fluorescence intensity and D) Paxillin proteins fluorescence intensity. E–G) Quantification of cell area, cell elongation, and circularity, respectively.

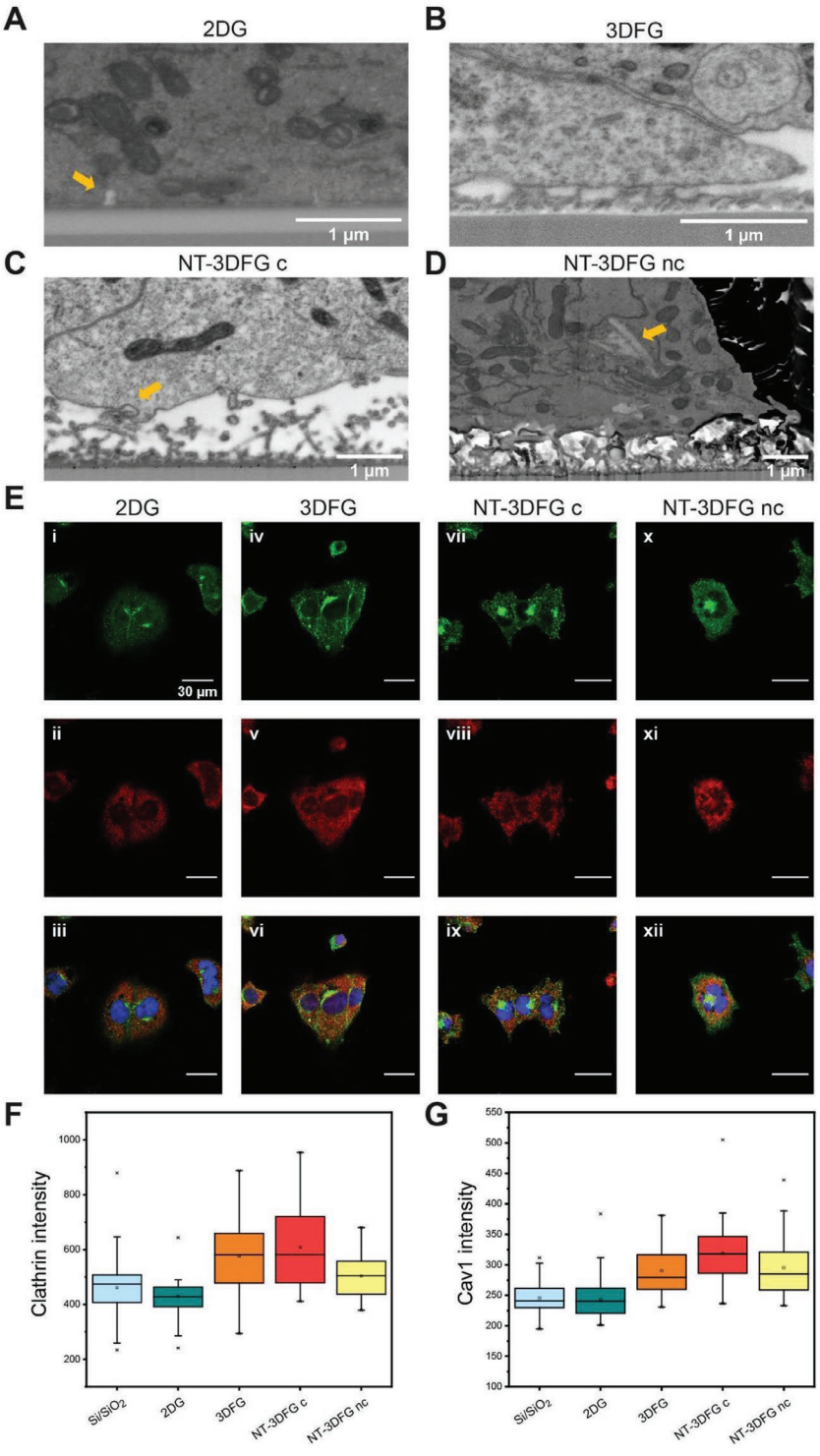

Figure 4. Membrane invagination as consequence of topographic cues. Scanning electron microscopy of A) 2DG graphene-cell cross section (tilt 52°, backscattered electrons), arrow identifies membrane invagination. B) 3DFG graphene-cell cross section (tilt 52°, backscattered electrons). C) NT-3DFG c-cell cross section (tilt 52°, backscattered electrons), arrow identifies membrane wrapping at single wire. D) NT-3DFG nc graphene-cell cross section (tilt 52°, backscattered electrons), arrow identifies a wire spontaneous penetration. E) Fluorescence images of cells on 2DG (i–iii), 3DFG (iv–vi), NT-3DFG c (vii–ix), and NT-3DFG nc (x–xii), where clathrin proteins were labeled in green, cav1 in red, and nuclei in blue. Quantification of F) clathrin fluorescence intensity and G) caveolin-1 fluorescence intensity.

Si/SiO_2). Notably, as result of the one-way ANOVA statistics ($p = 0.005$ as significance level), mean comparisons highlighted a statistically significant difference between the emitted signals from the planar cases (both 2DG and Si/SiO_2) and the out-of-plane ones (3DFG, NT-3DFGc, and NT-3DFGc). These measurements were consistent for both clathrin and cav-1. Therefore, the higher the fluorescence intensity the larger would be the number of endocytic vesicles, confirming the potential effect of out-of-plane graphene materials to provide local forces for specific membrane deformation and trigger intracellular recruitment of endocytic proteins. Regarding the spatial distribution, cav-1 vesicles were uniformly distributed across the whole cell body while the clathrin-mediated ones were highly localized near the nuclear region.

In summary, we have demonstrated that out-of-plane morphologies of graphene could be exploited in biomedical applications with electrogenic cells, since they do not noticeably alter cell viability or metabolic activity but rather gain more intimate contact with cells by promoting wrapping and engulfment-like events. Furthermore, these kinds of topographies might control on cytoskeleton assembly, FA proteins maturation as confirmed by fluorescence imaging. Cells interfaced with 3DFG developed a more organized actin network compared to the cells cultured on NT-3DFG templates. Similarly, FAs maturation was mostly impaired when cells were coupled with the structures with nanowire. Nevertheless, as SEM/FIB images revealed, cells' membrane has sufficient flexibility to tightly adhere on all out-of-plane graphene materials. Several freestanding wires in NT-3DFGnc template gain access to HL-1 cytosol, which might be related to a short-time penetration and subsequent membrane repair as no stable poration was detected.

Therefore, these results provide an enriched view of cell—nanotopography interaction and important insights into the design of protruding nanostructures (shape and size) to envision possible applications in bioelectronic and tissue engineering fields. On the one hand, 3DFG topography highlights the potential to be used for long-term stable culture, generally necessary to repristinate more closely cell natural conditions. On the other hand, both NT-3DFGc and nc designs might be suited for multifunctional purposes, such as electrical recording, stimulation, and delivery of molecules (i.e.,

therapeutic drugs), since the high spatial resolution achieved at single cells.

Experimental Section

Planar Graphene Synthesis: Monolayer graphene was synthesized using a Cu-catalyzed LPCVD process. A 2 cm × 6 cm Cu foil (99.8%, Alfa Aesar, uncoated) was cleaned with acetone in an ultrasonic bath for 5 min followed by isopropyl alcohol rinse and N_2 blow-dry. The Cu foil was pretreated with 5.4% w/w HNO_3 solution (CMOS Grade, J.T. Baker) for 30 s, rinsed twice with deionized (DI) water and N_2 blow-dried. The synthesis process was carried out at 1050 °C and 0.5 Torr. The temperature was ramped up to 1050 °C in 15 min, followed by stabilization at 1050 °C for 5 min under the flow of 100 standard cubic centimeters per minute (sccm) Ar. The foil was annealed for 60 min under H_2 flow of 100 sccm, followed by the synthesis step of 8 min under the flow of 50 sccm CH_4 (5% in Ar, Matheson Gas) and 100 sccm H_2 (Matheson Gas). The sample was rapidly cooled from growth temperature down to 100 °C in 30 min while flowing 100 sccm Ar. The Cu foil with graphene on both sides was cut into the desired dimensions. One side of the foil was coated with 200 nm of polymethylmethacrylate (PMMA 950 A4 MicroChem) to mechanically support the graphene and protect it from the subsequent steps. The foil was placed in a UV–ozone cleaner (PSD Pro series digital UV-Ozone, Novascan) and the graphene on the uncoated side was etched for 15 min at 150 °C. The Cu foil was wet-etched in a solution containing 25% w/w $FeCl_3.6H_2O$ (Sigma-Aldrich), 4% w/w HCl acid (CMOS grade, J.T. Baker), and 71% w/w DI water. At the end of the etching process the PMMA-supported graphene film was transferred to clean DI water for three times. Graphene-PMMA stack was transferred to a Si/SiO_2 sample (100) Si substrate with a 285 nm wet thermal oxide (p-type, 0.001–0.005 Ω cm, Nova Electronic Materials Ltd.). Prior to the graphene transfer, the substrates were cleaned with acetone in an ultrasonic bath for 5 min followed by isopropyl alcohol wash and N_2 blow-dry. The transferred sample was air-dried overnight. The substrate was then transferred in an oven at 150 °C for 30 min, followed by dissolving the PMMA in an acetone bath at 60 °C for 30 min. Finally, the samples were annealed at 300 °C for 1 h under 10 sccm H_2 at ambient pressure, to remove polymer impurities from the graphene surface.

3DFG Synthesis: 3DFG was synthesized using PECVD process. An induction coil was added to the quartz tube in the CVD system to generate inductively coupled plasma using a 13.56 MHz radiofrequency (RF) power supply (AG 0313 Generator and AIT-600 RF, power supply and auto tuner, respectively, T&C Power Conversion). A 1.5 cm × 1.5 cm Si/SiO_2 (100) Si substrate with a 600 nm wet thermal oxide (p-type, ≤0.005 Ω cm, Nova Electronic Materials Ltd.) sample was cleaned with acetone and isopropyl alcohol in an ultrasonic bath for 5 min each, and N_2 blow-dried. The substrate was placed onto a carrier wafer to position it at the center of the tube and was placed 4 cm from the edge of the RF coil. The temperature was ramped up to 800 °C in 13 min, followed by stabilization at 800 °C for 5 min, under a flow of 100 sccm Ar. The synthesis process was carried out for 30 min at 800 °C and 0.5 Torr under the flow of CH_4 with partial pressure of 25 mTorr. The plasma power was kept constant at 50 W. The plasma was shut down after the synthesis step and the sample was rapidly cooled from growth temperature to 100 °C in 30 min under 100 sccm Ar flow.

NT-3DFG Synthesis: SiNWs were synthesized by Au nanoparticles (AuNP) catalyzed vapor-liquid-solid growth process. Briefly, a 1.5 cm × 1.5 cm Si/SiO_2 sample (100) Si substrate with a 600 nm wet thermal oxide (p-type, ≤0.005 Ω cm, Nova Electronic Materials Ltd.) was cleaned with acetone and isopropyl alcohol in an ultrasonic bath for 5 min each, and N_2 blow-dried. The substrate was placed in a UV–ozone system (PSD Pro series digital UV-Ozone, Novascan) for 10 min at 150 °C. The substrate was then functionalized with 400 µL of 4:1 DI water:poly-L-lysine (PLL) (0.1% w/v, Sigma-Aldrich) for 8 min. Following this step, the substrate was gently washed three times in DI water and N_2 blow-dried. 30 nm AuNP solution (400 µL for 1.5 cm × 1.5 cm substrate, Ted Pella) was dispersed onto the PLL-coated substrate for 8 min. The substrate was gently washed three times in DI water, N_2 blow-dried, and introduced into a custom-built CVD setup. Once the baseline pressure of 1×10^{-5} Torr was reached, the temperature was ramped up to 450 °C in 8 min, followed by a 5 min stabilization step. Nucleation was conducted at 450 °C for 15 min with 80 sccm H_2 (Matheson Gas) and 20 sccm SiH_4 (10% in H_2, Matheson Gas) at 40 Torr. This was followed by a growth step under 60 sccm H_2, 20 sccm SiH_4, and 20 sccm PH_3 (1000 ppm in H_2, Matheson Gas) at 40 Torr for either 100 min (for collapsed NT-3DFG samples) or 5 min (for noncollapsed NT-3DFG samples). The sample was then rapidly cooled down to room temperature at base pressure.

For noncollapsed NT-3DFG samples, the 1.5 cm × 1.5 cm NW sample was introduced in the PECVD system, and 3DFG was synthesized as mentioned previously. Whereas for collapsed NT-3DFG samples, the synthesized NWs were collapsed by flowing liquid N_2 into the CVD quartz tube under 200 sccm Ar flow to form a NW mesh. The system was evacuated to base pressure followed by a 10 min mesh annealing step at 800 °C under 200 sccm H_2 flow at 1.6 Torr. Finally, the system was rapidly cooled to room temperature. The annealed samples were then introduced in the PECVD system followed by 3DFG synthesis.

SEM Imaging: SEM imaging was carried out using a FEI Quanta 600 field emission gun (FEG) SEM. The samples were imaged fixing the acceleration voltages in the range 5–20 kV and a working distance of 5 mm. The samples were not coated with a conductive coating prior to imaging.

Raman Spectroscopy: Raman spectroscopy was performed by NT-MDT NTEGRA Spectra (100× objective) using 532 nm excitation. Laser power of 2.38 mW was used, and the spectra were recorded with an acquisition time of 30 s. For G dispersion (Disp(G)) calculations, Raman spectra of each point were acquired using dual lasers: 532 and 633 nm (2.38 mW for both wavelengths).

Contact Angle Measurements: Contact angle measurements were performed with VCA optima (AST Products, Inc.) of DI water droplet (1.5 µL) injected onto the sample. The images were taken 5 s after the water droplet was dropped onto the sample surface. Contact angle values were determined with the use of AutoFAST Imaging Software (AST Products).

Preparation of Substrates for Cell Culture: Samples were sterilized under UV light for 60 min, right after being immersed and left in 70% ethanol for at least 60 min. The solution was then gradually replaced with DI water to make sure that ethanol solution was completely removed. Samples were functionalized prior to cells' plating to enhance their adhesion with a solution of 0.1% fibronectin (10 µL, Sigma-Aldrich), 0.2% porcine gelatin (100 µL), and sterilized water (1 mL). After at least 120 min of incubation at 37 °C, samples were rinsed with sterilized water and air-dried under a sterile hood before cell plating.

Cell Culture and Biocompatibility Assay: HL-1 cardiac muscle cells (Sigma-Aldrich) were cultured in Claycomb medium (Sigma-Aldrich) supplemented with 10% of fetal bovine serum (specific for HL-1 cell line, Merck Millipore), 1% of penicillin-streptomycin (10 000 U mL^{-1}, Sigma-Aldrich), 1% of GlutaMAX (Thermo Fisher Scientific), and 1% of noradrenaline.[31] Cells were gently seeded on each substrate at a density of 30 000 cells cm^{-2} and incubated at 37 °C with 5% CO_2. Cytotoxicity was evaluated after 1 DIV by fluorescently labeling alive and dead cells with Calcein-AM (Thermo Fisher Scientific) and propidium iodide (Thermo Fisher Scientific), respectively. Cells plated on to Si/SiO_2 substrate were set as negative control. The staining solution (1 µg mL^{-1} for Calcein AM and 10 µg mL^{-1} for propidium iodide) was added to cell media and incubated for 10 min. Samples were then rinsed in phosphate-buffered saline (PBS) and mounted on glass coverslip for imaging. Images were collected with epifluorescence microscope (Axio Observer Z1, Zeiss) using Planar Apocromat 20× 0.8 dry objective. % Viability quantification ($N = 3$) was evaluated using the following formula

$$\%\ \text{Viability} = \frac{\text{Live cells}}{(\text{Live cells} + \text{Dead cells})} \times 100 \quad (1)$$

Calcium Imaging: Functional assay of calcium wave propagation was performed after 1 DIV. Cells were first washed with PBS and then incubated at 37 °C with 5% CO_2 in Fluoro-4 AM (2×10^{-6} M, Invitrogen) solution in PBS for 30 min. Fluor-4 AM is a membrane-permeable dye and exhibits a large fluorescence intensity increase on binding free Ca^{2+}. After the incubation time, cells were washed in PBS and incubated again for 30 min with standard culture media prior acquisition. Finally, Ca^{2+} imaging was performed with an inverted microscope (Axio Vario, Zeiss) using an EC Plan-Neofluoar 10×/0.3 NA objective. The experimental tested window was set at 30 s. Ten experiments were carried out.

Calcium Wave Propagation Analysis: The acquired frames were processed computationally to obtain estimates of the calcium wave propagation velocities on each material type. The analysis process is summarized schematically, and the methodology is described in detail in Section S2 (Supporting Information). Briefly, the images were first scaled down and the frame-wide calcium wave events were identified as peaks in the mean intensity values across time. On the image series corresponding to each calcium wave event, the frame number of the intensity maxima of each pixel was used to form an image depicting the displacement of the wave in time. Detecting the edges on this image revealed the location of the wave front on each frame. The distance travelled by the wave was estimated based on the minimum distances between pixels corresponding to wave fronts in consecutive frames or time points. The propagation speed was subsequently computed diving the estimated travelled distance by the image acquisition period (0.056 s). The graph of Ca^{2+} propagation speed in function of normalized frequencies is shown in Figure S4 (Supporting Information).

Immunocytochemistry: Cells were fixed after 1 DIV in 4% paraformaldehyde (PAF) in PBS for 10 min at room temperature and then washed two times with PBS. Cells were permeabilized with 0.1% Triton-X 100 (Sigma-Aldrich) in PBS for 5 min and then blocked in 2% bovine serum albumin (BSA, Sigma-Aldrich) for 45 min at room temperature. Cells were labeled with Paxillin Monoclonal primary Antibody (5H11) (Thermo Fisher, Cat. No. AHO0492, 1:300 in 1% BSA in PBS) and added to the cells for 60–90 min at room temperature. Samples were then washed three times for 5 min in 1% BSA in PBS before being incubated with Alexa Fluor 488-labeled goat anti-mouse secondary antibody (1:1000, Thermo Fisher Scientific, Cat. No. A-11029) in 1% BSA in PBS for 60 min at room temperature; cells were then washed three times in 1% BSA in PBS. In addition, samples were also incubated with Phalloidin-X (1:1000 in 1% BSA in PBS, 555 nm as emission, Abcam) for 60 min at room temperature, following two washes in 1% BSA in PBS. Cell nuclei were stained with DRAQ5 (1:1000 in PBS, 695 as emission, Abcam) for 5 min at room temperature.

For clathrin and caveolin-1 labeling (mouse monoclonal [X22] to clathrin marker primary antibody (Cat. No. ab2731) and rabbit polyclonal to caveolin-1 marker primary antibodies (Cat. No. ab2910), respectively), both primary antibodies were diluted (1:500 in 1% BSA in PBS) and added to the cells for 40 min at room temperature. Samples were then washed three times for 5 min in 1% BSA in PBS before being incubated with Alexa Fluor 546-labeled goat anti-mouse and Alexa Fluor 488-labeled goat anti-rabbit secondary antibodies (anti-caveolin mouse 1:1000, 546 nm (Cat. No. A-11030) and anti-clathrin rabbit 1:1000, 488 nm) in 1% BSA in PBS for 60 min at room temperature; cells were then washed three times in 1% BSA in PBS.

All samples were stored upside down on a glass coverslip and shielded from light. A laser scanning confocal microscope (LSM 700, Carl Zeiss) was used for imaging using an apochromat 63×/1.4 NA oil immersion objective lens. All experiments were repeated three times for each material type. The fluorescence intensity measurements were explained in detail in Section S7 (Supporting Information).

Sample Preparation for Electron and Ion Microscopy: Cells on 2D and out-of-plane graphene were treated following the ultrathin plasticization.[18,19] First, samples were fixed in 2.5% glutaraldehyde (Electron Microscopy Science) diluted in sodium cacodylate buffer (0.1 M $C_2H_6AsNaO_2$, Electron Microscopy Science) for 60 min at room temperature and then washed three times for 5 min with buffer at 4 °C (samples should be held on ice). Afterward, the buffer was replaced with glycine (20×10^{-3} M) in $C_2H_6AsNaO_2$ solution (0.1 M) for 20 min at 4 °C and washed three times with buffer (5 min each). Specimens were incubated with 2% osmium tetroxide (Electron Microscopy Science) and 2% potassium ferrocyanide (Electron Microscopy Science) for 60 min at 4 °C and then washed three times with buffer solution. Afterward, samples were washed in DI water at room temperature and immersed in 1% filtered thiocarbohydrazide (TCH, Electron Microscopy Science) in DI water for 20 min at room temperature. TCH solution was washed three times with DI water for 5 min and subsequently replaced with 2% tetroxide osmium for 30 min at room temperature. Afterward, specimens were washed with DI water three times for 5 min and incubated overnight in 4% filtered uranyl acetate at 4 °C. Then, samples were washed three times with DI water and incubated with 0.15% tannic acid (Sigma-Aldrich) for 2 min at 4 °C and then washed two times with DI water. Dehydration was carried out in a series of ethanol dilutions (30, 50, 75, 95, 100% v/v ethanol in water) for 10 min at 4 °C. 100% ethanol was exchanged two times at room temperature and the specimens were then gradually embedded in resin (25 mL of NSA, 8 mL D.E.R. 736, 10 mL of ERL 4221, 301 µL of DMAE, Electron Microscopy Science) with an ethanol:resin ratio (1:3 for 3 h, 1:1 overnight, absolute resin for at least other 8 h). Finally, resin was polymerized in the oven at 70 °C for 12 h. Samples were mounted onto aluminum pin stubs (diam. 3.2 mm) using silver conductive paste (RS Pro) and sputtered with 5 nm thick golden layer prior imaging.

Scanning Electron Microscopy and Focused Ion Beam Milling: Samples were loaded inside the dual-beam chamber (Thermo Fisher, Helios NanoLab 600i and 650) and a region of interest (ROI) was located. Platinum was deposited in two steps at ROI following an electron-assisted deposition (0.5 µm thickness at 3 kV and 0.69–2.7 nA) and a subsequent ion-assisted deposition (≈1 µm thickness at 30.0 kV and 0.79 nA). Cross sections were realized by first trenching out the material via ion beam (≈5 µm nominal depth for Si 30.0 kV and 0.25–9.3 nA) and then by polishing the interface with the ion beam (≈1 µm nominal depth for Si, 30.0 kV and 80 pA to 0.23 nA). Scanning electron microscopy images were acquired in backscattered mode fixing dwell time at 30 µs and the electron beam parameters to 2.0 kV and 86 pA to 2.8 nA.

Supporting Information

Supporting Information is available from the Wiley Online Library or from the author.

Acknowledgements

The authors thank V. Mollo for the preparation of SEM/FIB samples and A. Qualtieri for help with SEM-FIB at the IIT Center for Biomolecular Nanotechnologies in Lecce and the Cleanroom Facility at the IIT Center for Convergent Technologies in Genoa, Italy. T.C.-K. acknowledges funding support from the National Science Foundation under Award No. CBET1552833 and the Office of Naval Research under Award No. N000141712368. T.C.-K. and S.K.R. also acknowledge support from the Department of Materials Science and Engineering Materials Characterization Facility (MCF-677785).

Conflict of Interest

The authors declare no conflict of interest.

Keywords

bioelectronics, biointerfaces, biomaterials, graphene, out-of-plane structures, SEM/FIB

Received: April 22, 2020
Revised: June 10, 2020
Published online:

[1] F. A. Pennacchio, L. D. Garma, L. Matino, F. Santoro, *J. Mater. Chem. B* **2018**, *6*, 7096.
[2] M. E. Spira, D. Kamber, A. Dormann, A. Cohen, C. Bartic, G. Borghs, J. P. M. Langedijk, S. Yitzchaik, K. Shabthai, J. Shappir, in *TRANSDUCERS 2007 – 2007 Int. Solid-State Sensors, Actuators and Microsystems Conf.*, IEEE, Piscataway, NJ **2007**, pp. 1247–1250.
[3] K. Toma, H. Kano, A. Offenhäusser, *ACS Nano* **2014**, *8*, 12612.
[4] A. F. McGuire, F. Santoro, B. Cui, *Annu. Rev. Anal. Chem.* **2018**, *11*, 101.
[5] Y. Cao, S. Cong, X. Cao, F. Wu, Q. Liu, R. A. Moh, C. Zhou, in *Single-Walled Carbon Nanotubes: Preparation, Properties and Applications*, Topics in Current Chemistry Collections, Vol. *377* (Eds: Y. Li, S. Maruyama), Springer International Publishing, Cham, Switzerland **2019**, pp. 189–224.
[6] C. Chung, Y.-K. Kim, D. Shin, S.-R. Ryoo, B. H. Hong, D.-H. Min, *Acc. Chem. Res.* **2013**, *46*, 2211.
[7] S. K. Rastogi, A. Kalmykov, N. Johnson, T. Cohen-Karni, *J. Mater. Chem. B* **2018**, *6*, 7159.
[8] A. Kalmykov, C. Huang, J. Bliley, D. Shiwarski, J. Tashman, A. Abdullah, S. K. Rastogi, S. Shukla, E. Mataev, A. W. Feinberg, K. J. Hsia, T. Cohen-Karni, *Sci. Adv.* **2019**, *5*, eaax0729.
[9] D. Kireev, M. Brambach, S. Seyock, V. Maybeck, W. Fu, B. Wolfrum, A. Offenhäusser, *Sci. Rep.* **2017**, *7*, 6658.
[10] D. Kireev, S. Seyock, J. Lewen, V. Maybeck, B. Wolfrum, A. Offenhäusser, *Adv. Healthcare Mater.* **2017**, *6*, 1601433.
[11] N. P. Pampaloni, M. Lottner, M. Giugliano, A. Matruglio, F. D'Amico, M. Prato, J. A. Garrido, L. Ballerini, D. Scaini, *Nat. Nanotechnol.* **2018**, *13*, 755.
[12] S. K. Rastogi, G. Raghavan, G. Yang, T. Cohen-Karni, *Nano Lett.* **2017**, *17*, 3297.
[13] R. Garg, S. K. Rastogi, M. Lamparski, S. C. de la Barrera, G. T. Pace, N. T. Nuhfer, B. M. Hunt, V. Meunier, T. Cohen-Karni, *ACS Nano* **2017**, *11*, 6301.
[14] A. C. Ferrari, D. M. Basko, *Nat. Nanotechnol.* **2013**, *8*, 235.
[15] A. B. D. Cassie, S. Baxter, *Trans. Faraday Soc.* **1944**, *40*, 546.
[16] X.-M. Li, D. N. Reinhoudt, M. Crego-Calama, *ChemInform* **2007**, *38*.
[17] S. K. Rastogi, J. Bliley, L. Matino, R. Garg, F. Santoro, A. W. Feinberg, T. Cohen-Karni, *Nano Res.* **2020**, *13*, 1444.
[18] X. Li, L. Matino, W. Zhang, L. Klausen, A. F. McGuire, C. Lubrano, W. Zhao, F. Santoro, B. Cui, *Nat. Protoc.* **2019**, *14*, 1772.
[19] F. Santoro, W. Zhao, L.-M. Joubert, L. Duan, J. Schnitker, Y. van de Burgt, H.-Y. Lou, B. Liu, A. Salleo, L. Cui, Y. Cui, B. Cui, *ACS Nano* **2017**, *11*, 8320.
[20] C. A. Heckman, H. K. Plummer, *Cell. Signalling* **2013**, *25*, 2298.
[21] Y.-S. Park, S. Y. Yoon, J. S. Park, J. S. Lee, *NPG Asia Mater.* **2016**, *8*, e249.
[22] M. J. Dalby, M. O. Riehle, H. Johnstone, S. Affrossman, A. S. G. Curtis, *Cell Biol. Int.* **2004**, *28*, 229.
[23] W. Zhao, L. Hanson, H.-Y. Lou, M. Akamatsu, P. D. Chowdary, F. Santoro, J. R. Marks, A. Grassart, D. G. Drubin, Y. Cui, B. Cui, *Nat. Nanotechnol.* **2017**, *12*, 750.
[24] H.-Y. Lou, W. Zhao, X. Li, L. Duan, A. Powers, M. Akamatsu, F. Santoro, A. F. McGuire, Y. Cui, D. G. Drubin, B. Cui, *Proc. Natl. Acad. Sci. USA* **2019**, *116*, 23143.
[25] C. S. Hansel, S. W. Crowder, S. Cooper, S. Gopal, M. João Pardelha da Cruz, L. de Oliveira Martins, D. Keller, S. Rothery, M. Becce, A. E. G. Cass, C. Bakal, C. Chiappini, M. M. Stevens, *ACS Nano* **2019**, *13*, 2913.
[26] H.-Y. Lou, W. Zhao, Y. Zeng, B. Cui, *Acc. Chem. Res.* **2018**, *51*, 1046.
[27] M. J. P. Biggs, R. G. Richards, M. J. Dalby, *Nanomed.: Nanotechnol., Biol. Med.* **2010**, *6*, 619.
[28] S. Gopal, C. Chiappini, J. Penders, V. Leonardo, H. Seong, S. Rothery, Y. Korchev, A. Shevchuk, M. M. Stevens, *Adv. Mater.* **2019**, *31*, 1806788.
[29] F. A. Pennacchio, F. Caliendo, G. Iaccarino, A. Langella, V. Siciliano, F. Santoro, *Nano Lett.* **2019**, *19*, 5118.
[30] M. Galic, S. Jeong, F.-C. Tsai, L.-M. Joubert, Y. I. Wu, K. M. Hahn, Y. Cui, T. Meyer, *Nat. Cell Biol.* **2012**, *14*, 874.
[31] W. C. Claycomb, N. A. Lanson, B. S. Stallworth, D. B. Egeland, J. B. Delcarpio, A. Bahinski, N. J. Izzo, *Proc. Natl. Acad. Sci. USA* **1998**, *95*, 2979.

